

A HYBRID MODEL FOR TRAFFIC FLOW AND CROWD DYNAMICS WITH RANDOM INDIVIDUAL PROPERTIES

VERONIKA SCHLEPER

Institute for Applied Analysis and Numerical Simulation
University of Stuttgart
D-70569 Stuttgart, Germany

ABSTRACT. Based on an established mathematical model for the behavior of large crowds, a new model is derived that is able to take into account the statistical variation of individual maximum walking speeds. The same model is shown to be valid also in traffic flow situations, where for instance the statistical variation of preferred maximum speeds can be considered. The model involves explicit bounds on the state variables, such that a special Riemann solver is derived that is proved to respect the state constraints. Some care is devoted to a valid construction of random initial data, necessary for the use of the new model. The article also includes a numerical method that is shown to respect the bounds on the state variables and illustrative numerical examples, explaining the properties of the new model in comparison with established models.

1. Introduction. Since many years, increasing attention is given to the modeling and simulation of traffic flow and crowd dynamics - two phenomena that are closely related from a modeling point of view. Starting in the 1950s, first continuum models for traffic flow appeared, see [15, 17]. Subsequently, more refined models based on fluid dynamical approaches appeared, but suffered from a severe drawback of information reaching drivers from behind, see [9, 2, 12] for a discussion of this problem and new approaches to overcome this inconsistency. More recent are approaches to continuum modeling of crowd dynamics and pedestrian flows, see e.g. [13, 3, 5] and the review article [4].

As already addressed in [9], vehicles (and pedestrians) are not uniform particles, but have individual properties, such as different braking behavior or individual maximum speeds. This fact is also addressed in a recent review article [4], where the authors remind that more care should be devoted to the right choice of scales. Especially, they point out some important points that should be taken into account during the modeling approach. Among others, they state that

1. The systems are discrete with finite degrees of freedom, but models should allow for the evaluation of macroscopic quantities.
2. The number of individuals in the system is not large enough to allow the use of continuous distributions.
3. The interactions of individuals are not localized to the point where the individual is at the moment, but are adjusted to the traffic conditions in front.

2010 *Mathematics Subject Classification.* Primary: 35L40, 35L65, 90B20, 35R60.

Key words and phrases. Crowd dynamics, traffic flow, non-local conservation laws, random initial data.

While the property of item 3. is addressed by recent models for traffic and pedestrian flows (see e.g. [13, 1, 3, 5, 11]), there are only few approaches that are able to take into account at least part of the suggestions of items 1. and 2., see e.g. [8, 6] where micro- and macroscale dynamics are combined.

In the following, we propose a new model, that can be seen as a hybrid system, taking into account the macroscopic behavior of cars or pedestrians, but allowing for some individual properties that are transported with the flow. In this presentation, we limit the individual property on a variation of the maximum speed or the speed law respectively. However, the model generally allows also for the inclusion of other individual properties, while the additional costs amount only in the tracking of the individual property, what can be numerically performed by suitable convex combinations.

Although we focus on applications related to crowd dynamics and traffic flow, the general idea of hybrid models, containing macroscopic dynamics and individual properties, can be directly transferred to a wide class of models, especially related to biological applications, where individual differences play important roles in the behaviour and evolution of the systems. The reason to focus on the two aforementioned applications lies in the fact that the macroscopic equations are relatively simple and well understood. This allows us to clearly see and state the important new features of the hybrid model.

Due to the fact that we allow for individual properties, the question of valid initial data arises. Therefore, we propose also a method to generate random initial data for the new model, based on the underlying modeling context.

The model is based on the deterministic non-local crowd dynamics model, proposed in [13, 5], given by

$$\partial_t \rho + \mathbf{div} (\rho v(\rho) (\boldsymbol{\nu}(\mathbf{x}) - \varepsilon \mathcal{I}(\nabla \eta * \rho))) = 0. \quad (1)$$

For this conservation law, existence and uniqueness of weak entropy solutions to the Cauchy problem in several space dimensions are provided in [5], see also section 4 for a short review of these results. The above model implies that all persons move according to the same speed law $v(\rho)$. The desired direction $\boldsymbol{\nu}(\mathbf{x})$ is modified by a nonlocal term \mathcal{I} , involving a weighted average of the pedestrian density around point x at time t . This modification has the effect that individuals approaching a zone of higher density try to avoid this region by deviating from their shortest paths.

In reality, the assumption of equal maximum speed is not true. Especially the maximum speed $\max_\rho v(\rho)$ of two persons differs by reasons of e.g. age, occupation and target. Persons, on their way to work will for instance try to walk faster even in high density traffic conditions than individuals walking their dogs or talking to peers. To take into account the different maximum walking speeds, we propose a modified version of (1), which we will call α -model in the following.

$$\partial_t \rho + \mathbf{div} (\rho \mathbf{V}(\rho, \alpha, x)) = 0 \quad (2a)$$

$$\partial_t \alpha + \mathbf{V}(\rho, \alpha, x) \cdot \nabla \alpha = 0 \quad (2b)$$

$$\mathbf{V}(\rho, \alpha, x) = v(\rho, \alpha) (\boldsymbol{\nu}(x) - \varepsilon \mathcal{I}(\nabla \eta * \rho)) \quad (2c)$$

$$0 \leq \rho \leq \rho_{\max} \quad \alpha_{\min} \leq \alpha \leq \alpha_{\max} \quad (2d)$$

Hereby, $\alpha(t, x)$ denotes the maximal speed of the person located in position x at time t . Once $\alpha(0, x)$ is chosen, it is transported with the flow by equation (2b) and can therefore be seen as a characteristic value moving with the respective person

along the path specified by the velocity field $\mathbf{V}(\rho, \alpha, x)$. Since we do not have a maximum principle for systems of conservation laws, we impose the boundedness of density and maximal velocities in (2d). In Section 2.1, we show that (at least in one space dimension) the bound on α is automatically fulfilled by the solution, while the lower bound on ρ is necessary to avoid negative densities.

For the speed laws $v(\rho)$ and $v(\rho, \alpha)$, we impose the following condition.

- (v) $v \in \mathbf{C}^2(\mathbb{R}, \mathbb{R})$ is non-increasing and fulfills $v(0) = v_{\max}$ and $v(\rho_{\max}) = 0$ for fixed $v_{\max} \in \mathbb{R}$ and $\rho_{\max} \in \mathbb{R}^+$.
- (v $_{\alpha}$) $v \in \mathbf{C}^2(\mathbb{R} \times \mathbb{R}^+, \mathbb{R})$ is non-increasing in the first variable and non-decreasing in the second variable and fulfills $v(0) = \alpha$ and $v(\rho_{\max}) = 0$ for fixed $\rho_{\max} \in \mathbb{R}^+$.

This assures that the velocity decreases with increasing density and that any movement breaks down at maximum density. Examples for possible choices of the speed law $v(\rho, \alpha)$ are for instance given by one of the following functions

$$v(\rho, \alpha) = \alpha \left(1 - \frac{\rho}{\rho_{\max}}\right), \quad v(\rho, \alpha) = \min\{v_{\max}, \alpha\} \left(1 - \frac{\rho}{\rho_{\max}}\right), \quad (3)$$

see also Figure 1.

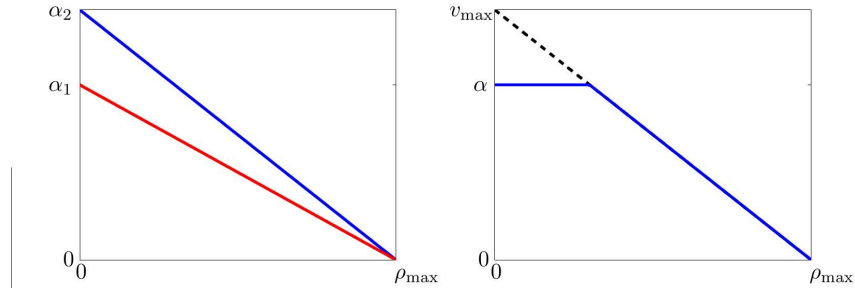


FIGURE 1. Illustration of two possible choices of individual speed laws. The left choice uses different slopes for different values of α , while the right version uses the same slope, but is cut off at the maximal speed α .

In a more general setting, we can write model (2) in the form

$$\partial_t \rho + \operatorname{div}(\rho \mathcal{V}(\rho, \alpha, x, t)) = 0 \tag{4a}$$

$$\partial_t \alpha + \mathcal{V}(\rho, \alpha, x, t) \cdot \nabla \alpha = 0 \tag{4b}$$

$$0 \leq \rho \leq \rho_{\max} \quad 0 < \alpha_{\min} \leq \alpha \leq \alpha_{\max} \tag{4c}$$

in a domain $\mathcal{D} \subset \mathbb{R}^d$. This setting also covers the case of traffic flow, where we assign different values of maximal speed to different cars or drivers. In this case, we can choose $\mathcal{V}(\rho, \alpha, x, t) = v(\rho, \alpha)$, for $v(\rho, \alpha)$ such that (v $_{\alpha}$) is fulfilled. Possible choices of $v(\rho, \alpha)$ in the case of traffic flow include the examples given in (3). In section 2, we show that the α -model for traffic flow is able to reproduce the sudden appearance of zones of higher traffic density, even when we start with homogeneous initial density (see [19, 20] for empirical studies of this phenomenon). These regions of higher traffic density turn out to be the result of small differences in the maximal speed of the cars.

Note that in [1], also nonlocal choices for $\mathcal{V}(\rho, \alpha, x, t)$ are proposed, similar to the case of crowd dynamics. However, the local model is more common in traffic simulations, so that we chose to focus on the local model for traffic flow and show the behavior of the nonlocal case only for pedestrian movements.

The paper is organized as follows. In section 2, we discuss the one dimensional Riemann problem for a local version of (4) and present a finite volume method for its numerical treatment. We show that the numerical scheme respects the bounds on ρ and α imposed by (4c) and present numerical examples explaining the effect of the additional variable α . It can be seen from the results, that the inclusion of α produces a much more realistic behavior of the solution than the standard Lighthill-Witham-Richards (LWR) model (see [15]).

Section 3 is devoted to the generation of random initial data for ρ and α . Here especially the generation of random data for the initial density distribution is inspired by the underlying modeling context, since we cannot define probability spaces on (a subset of) infinite dimensional spaces like $\mathbf{L}^1(\mathcal{D})$. The construction of random initial data will then be used to compare the α -model (2) and the standard model (1) in an evacuation scenario in section 4.

2. Results on the α -model in one space dimension.

2.1. The Riemann solver for the one dimensional case. To allow a deeper understanding of the structure of solutions to the α -model, we derive some results on the one dimensional case first. To this end, consider the following system of conservation laws in one space dimension.

$$\partial_t \rho + \partial_x (\rho v(\rho, \alpha)) = 0 \quad (5a)$$

$$\partial_t \alpha + v(\rho, \alpha) \partial_x \alpha = 0 \quad (5b)$$

$$v(\rho, \alpha) = \alpha(1 - \rho) \quad (5c)$$

$$0 \leq \rho \leq 1 \quad 0 < \alpha_{\min} \leq \alpha \leq \alpha_{\max} \quad (5d)$$

Here and in the following we assume $\rho_{\max} = 1$, which can be obtained from 4 by scaling. Denoting $\mathbf{u} := (\rho, \alpha)^T$ and $f(\mathbf{u}) := \rho v(\rho, \alpha)$, we see that the Jacobi matrix of the above system

$$A = \begin{pmatrix} v(\rho, \alpha) - \alpha\rho & \rho(1 - \rho) \\ 0 & v(\rho, \alpha) \end{pmatrix}$$

admits two real eigenvalues

$$\lambda_1(\rho, \alpha) = v(\rho, \alpha) - \alpha\rho \quad \text{and} \quad \lambda_2(\rho, \alpha) = v(\rho, \alpha)$$

with corresponding eigenvectors

$$\mathbf{r}_1 = \begin{pmatrix} 1 \\ 0 \end{pmatrix} \quad \text{and} \quad \mathbf{r}_2 = \begin{pmatrix} 1 - \rho \\ \alpha \end{pmatrix}.$$

From these eigenvalue-eigenvector pairs it is obvious that $\lambda_1(\rho, \alpha) \leq \lambda_2(\rho, \alpha)$ and system (5) is strictly hyperbolic as long as $\rho > 0$, that is as long as no vacuum occurs.

We proceed now by studying the wave structure of the solution to Riemann problems, i.e. to (5) with initial conditions of the form

$$(\rho, \alpha)(0, x) = \begin{cases} (\rho_-, \alpha_-) & x \leq 0 \\ (\rho_+, \alpha_+) & x > 0 \end{cases}. \quad (6)$$

From the eigenvalue-eigenvector pairs, we deduce

$$\nabla_{\mathbf{u}}\lambda_1(\mathbf{u}) \cdot \mathbf{r}_1 = -2\alpha \qquad \nabla_{\mathbf{u}}\lambda_2(\mathbf{u}) \cdot \mathbf{r}_2 = 0.$$

The first wave family is therefore genuinely nonlinear, while the second family is linear degenerate, thus producing only contact discontinuities. Since system (5) consists of one conservative and one non-conservative equation, we have to follow arguments similar to those in [10] to give a meaning to the non-conservative product $v(\rho, \alpha)\partial_x\alpha$. Since the second wave family is linearly degenerate, we deduce that the velocity satisfies $v(\tilde{\rho}, \tilde{\alpha}) = v(\rho_+, \alpha_+)$, where $(\tilde{\rho}, \tilde{\alpha})$ is the middle state to be determined. From a modeling point of view it is furthermore reasonable to assume that $\tilde{\alpha} = \alpha_-$. This guarantees that the driver does not change his maximum desired speed during interactions with other drivers and implies that the solution coincides with the classical LWR solution if $\alpha_+ = \alpha_-$. Note that the choice of $(\tilde{\rho}, \alpha_-)$ as middle state allows to define a path Φ that satisfies the requirements of the results in [10] and thus yields a well-posed definition of the non-conservative product.

The two possible wave structures of a solution to the Riemann problem (5), (6) are illustrated in Figure 2.

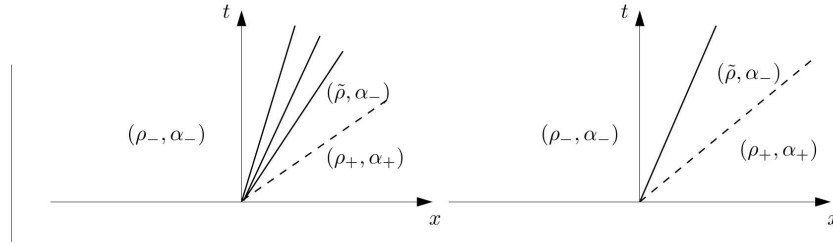


FIGURE 2. Illustration of the two wave patterns that can arise in the solution of Riemann problems of system (5). Left: Rarefaction wave (solid) and contact discontinuity (dashed). Right: Shock wave (solid) and contact discontinuity (dashed).

As stated above, denoting by s_2 the speed of the contact discontinuity, it is easy to see that the solution across such a contact discontinuity has to fulfill

$$s_2 = v(\rho_+, \alpha_+) = v(\tilde{\rho}, \alpha_-).$$

From $v(\rho_+, \alpha_+) = v(\tilde{\rho}, \alpha_-)$, we can therefore deduce

$$v(\rho_+, \alpha_+) = \alpha_-(1 - \tilde{\rho})$$

and thus

$$\tilde{\rho} = 1 - \frac{v(\rho_+, \alpha_+)}{\alpha_-} = \rho_- + \frac{1}{\alpha_-} (v(\rho_-, \alpha_-) - v(\rho_+, \alpha_+)).$$

Obviously, we have $\tilde{\rho} > 0$ as long as $v(\rho_+, \alpha_+) < \alpha_-$. This implies especially that the model allows the appearance of vacuum states also for initial data away from vacuum. We will see below, that this is the case only for strong rarefaction waves. In case of negative values of $\tilde{\rho}$, we have to modify the solution of the Riemann problem to respect the lower bound on ρ imposed by the model in (2d), see Case 2b below.

With this in mind, we can now give the exact solution to the Riemann problem, depending on the relation of the initial velocities $v(\rho_-, \alpha_-)$ and $v(\rho_+, \alpha_+)$.

Case 1. $v(\rho_-, \alpha_-) > v(\rho_+, \alpha_+)$, $\rho_- > 0, \rho_+ > 0$. In this case, the solution consists of a shock wave, connecting (ρ_-, α_-) and $(\tilde{\rho}, \alpha_-)$ followed by a contact discontinuity connecting $(\tilde{\rho}, \alpha_-)$ and (ρ_+, α_+) . Note that we obtain $\rho_- \leq \tilde{\rho} \leq 1$ for all choices of (ρ_+, α_+) and (ρ_-, α_-) fulfilling the Case 1 condition on the velocity. To determine the speed s_1 of the shock wave, we note that α is constant across waves of the first family. Therefore, we require that ρ fulfills the standard Rankine-Hugoniot jump condition for the conservative equation (5a), yielding

$$s_1 = \alpha_- \frac{\tilde{\rho}(1 - \tilde{\rho}) - \rho_-(1 - \rho_-)}{\tilde{\rho} - \rho_-}$$

such that the solution is given by

$$\rho(t, x) = \begin{cases} \rho_- & \text{if } x \leq s_1(\rho_-, \alpha_-)t \\ \tilde{\rho} & \text{if } s_1 t < x \leq v(\rho_+, \alpha_+)t, \\ \rho_+ & \text{if } v(\rho_+, \alpha_+)t < x \end{cases}$$

$$\alpha(t, x) = \begin{cases} \alpha_- & \text{if } x \leq v(\rho_+, \alpha_+)t \\ \alpha_+ & \text{if } v(\rho_+, \alpha_+)t < x \end{cases}.$$

Case 2a. $v(\rho_-, \alpha_-) \leq v(\rho_+, \alpha_+) \leq \alpha_-$, $\rho_- > 0, \rho_+ > 0$. In this case, the solution consists of a rarefaction wave of the first wave family and a contact discontinuity of the second wave family. Using the self similarity of solutions to the Riemann problem, we can explicitly compute the rarefaction wave in the solution and obtain

$$\rho(t, x) = \begin{cases} \rho_- & \text{if } x \leq \lambda_1(\rho_-, \alpha_-)t \\ \rho_- - \frac{1}{2\alpha_-} \left(\frac{x}{t} - \lambda_1(\rho_-, \alpha_-) \right) & \text{if } \lambda_1(\rho_-, \alpha_-)t < x \leq \lambda_1(\tilde{\rho}, \alpha_-)t \\ \tilde{\rho} & \text{if } \lambda_1(\tilde{\rho}, \alpha_-)t \leq x \leq v(\rho_+, \alpha_+)t \\ \rho_+ & \text{if } v(\rho_+, \alpha_+)t < x \end{cases},$$

$$\alpha(t, x) = \begin{cases} \alpha_- & \text{if } x \leq v(\rho_+, \alpha_+)t \\ \alpha_+ & \text{if } v(\rho_+, \alpha_+)t < x \end{cases}.$$

Thus, the rarefaction wave connects the states (ρ_-, α_-) and $(\tilde{\rho}, \alpha_-)$ and is followed by the contact discontinuity connecting $(\tilde{\rho}, \alpha_-)$ and (ρ_+, α_+) . The condition $v(\rho_+, \alpha_+) \leq \alpha_-$ now assures that $\tilde{\rho} \geq 0$, and therefore $\rho(t, x) \geq 0$ for all (t, x) and $\rho(t, x) = 0$ only when $\lambda_1(\tilde{\rho}, \alpha_-) \leq x \leq v(\rho_+, \alpha_+)t$ and $v(\rho_+, \alpha_+) = \alpha_+$.

Case 2b. $v(\rho_-, \alpha_-) \leq v(\rho_+, \alpha_+)$, $v(\rho_+, \alpha_+) > \alpha_-$, $\rho_- > 0, \rho_+ > 0$. In this case, we also expect a rarefaction wave followed by a contact discontinuity connecting the initial states (ρ_-, α_-) and (ρ_+, α_+) . But contrary to Case 2a above, this case yields $\tilde{\rho} < 0$. This indicates that we have to modify the solution of the Riemann problem to guarantee that $\rho(t, x)$ remains non-negative in the whole computational domain.

Note that system (5) is no longer hyperbolic as soon as vacuum states appear. Especially, it is not clear any more if we have a unique solution involving vacuum states. This gives some freedom in the choice of modification we can perform to guarantee the lower bound on ρ . We therefore choose to cut off the rarefaction wave

once $\rho_- - \frac{1}{\alpha_-} \left(\frac{x}{t} - v(\rho_-, \alpha_-) \right) = 0$, i.e. we set the solution $\rho(t, x) = 0$ in the interval $\alpha_- t \leq x \leq v(\rho_+, \alpha_+)$.

$$\rho(t, x) = \begin{cases} \rho_- & \text{if } x \leq \lambda_1(\rho_-, \alpha_-)t \\ \rho_- - \frac{1}{2\alpha_-} \left(\frac{x}{t} - \lambda_1(\rho_-, \alpha_-) \right) & \text{if } \lambda_1(\rho_-, \alpha_-)t < x < \alpha_- t \\ 0 & \text{if } \alpha_- t \leq x \leq v(\rho_+, \alpha_+) \\ \rho_+ & \text{if } v(\rho_+, \alpha_+)t < x \end{cases},$$

This procedure unfortunately introduces a new problem, since now the state to the left of the contact discontinuity $(0, \alpha_-)$ does not fulfill the jump condition $v(\rho_+, \alpha_+) = \alpha_-(1 - \rho_-) = \alpha_-$. However, this is only a formal problem, since an empty space does not contain any car, and therefore α is formally not defined there. Therefore, we impose the additional condition that *an empty space to the left (i.e. behind the car) does not influence the driver’s behavior*, see Case 3 below for more details on solutions with vacuum states. This means that we simply define the following structure of α

$$\alpha(t, x) = \begin{cases} \alpha_- & \text{if } x \leq v(\rho_+, \alpha_+)t \\ \alpha_+ & \text{if } v(\rho_+, \alpha_+)t < x \end{cases}.$$

Formally, the solution to the Riemann problem in Case 2b is thus composed of two waves: one rarefaction wave, connecting (ρ_-, α_-) and $(0, \alpha_-)$, and a contact discontinuity, connecting $(0, \alpha_+)$ and (ρ_+, α_+) . The latter does formally not fulfill the jump condition required for contact discontinuities, but this condition does not hold in vacuum situations. Instead we can interpret the jump from $(0, \alpha_-)$ to (ρ_+, α_+) as the result of the fusion of a wave of the first family and a contact discontinuity, since their speeds coincide at vacuum states. The special structure of this solver results from the positivity constraint in the model (5).

Case 3. $\rho_- > 0, \rho_+ = 0$. We consider now the case that a car faces an empty region. In that case, we cannot uniquely¹ assign any value of α to the empty region, since α is a property attached to a car (no car - no individual properties). Furthermore, since the system is not hyperbolic in the presence of vacuum, the solution of the Riemann problem is no longer unique and we have to *choose* how the solution should behave.

From a modeling point of view, it is natural to assume that the car starts to accelerate until it reaches its maximal speed. To assure that this is possible, we formally assign $\alpha_+ := \alpha_{\max}$, thus assuming that any car in the empty region would travel as fast as possible. Comparing the resulting velocities, we obtain $v(\rho_-, \alpha_-) = \alpha_-(1 - \rho_-) < \alpha_- \leq \alpha_{\max} = v(\rho_+, \alpha_+)$. Analogously to Case 2b, the solution is therefore given by a rarefaction wave connecting (ρ_-, α_-) and $(0, \alpha_-)$ and a contact discontinuity, connecting $(0, \alpha_-)$ and $(0, \alpha_{\max})$.

$$\rho(t, x) = \begin{cases} \rho_- & \text{if } x \leq \lambda_1(\rho_-, \alpha_-)t \\ \rho_- - \frac{1}{2\alpha_-} \left(\frac{x}{t} - \lambda_1(\rho_-, \alpha_-) \right) & \text{if } \lambda_1(\rho_-, \alpha_-)t < x \leq \alpha_- t, \\ 0 & \text{if } \alpha_- t < x \end{cases}$$

¹This non-uniqueness is different from the well-known non-uniqueness of solutions involving non-conservative products, as it occurs even once a path is defined that guarantees the well-posed definition of the non-conservative product.

$$\alpha(t, x) = \begin{cases} \alpha_- & \text{if } x \leq \alpha_- t \\ \alpha_{\max} & \text{if } \alpha_- t < x \end{cases}.$$

Case 4. $\rho_- = 0, \rho_+ > 0$. In this case, an empty space occurs *behind* the car. From a modeling point of view it is natural to assume that the car is not affected by events from behind, especially not from empty space behind. In the present case, this means that we impose that the solution to the α -model coincides with the solution of the standard LWR model. Therefore, we proceed as in Case 2b and define the solution by

$$\begin{aligned} \rho(t, x) &= \begin{cases} 0 & \text{if } x \leq v(\rho_+, \alpha_+)t \\ \rho_+ & \text{if } b(\rho_+, \alpha_+)t < x \end{cases}, \\ \alpha(t, x) &= \begin{cases} \alpha_{\max} & \text{if } x \leq v(\rho_+, \alpha_+)t \\ \alpha_+ & \text{if } v(\rho_+, \alpha_+)t < x \end{cases}. \end{aligned}$$

Case 5. $\rho_- = 0, \rho_+ = 0$. Again, we impose that the solution must coincide with the solution of the standard LWR model (5a) with $v(\rho) = v(\rho, \bar{\alpha}) = \bar{\alpha}(1 - \rho)$ for some arbitrary fixed $\bar{\alpha} > 0$. The solution thus remains trivial, i.e.

$$\rho(t, x) = 0 \quad \text{and} \quad \alpha(t, x) = \bar{\alpha}.$$

Note that the above procedure assures that the bounds on ρ and α in (5d) are respected. However, the Riemann solver constructed above seems to be *not* continuously depending on the initial data as soon as vacuum appears. Therefore, the standard results on existence, uniqueness and continuous dependence of solutions to the Cauchy problem do not apply to the present case, making further investigations in this direction necessary.

2.2. A finite volume method for the one-dimensional case. To solve (5) numerically, we propose a finite volume method, based on the above described Riemann solver. Thus, we choose an (equidistant) space grid $\{x_i\}_{i=-\infty}^{\infty}$ and a corresponding time grid $\{t^n\}_{n=0}^N$ with grid constants $h = x_i - x_{i-1}$ and $k = t_i - t_{i-1}$ and approximate the initial data $u(0, x) := (\rho(0, x), \alpha(0, x))^T$ by the integral mean of each grid cell $[x_{i-1/2}, x_{i+1/2}]$:

$$u_i^0 = \frac{1}{h} \int_{x_{i-1/2}}^{x_{i+1/2}} u(0, x) dx. \quad (7)$$

Using this approximation, the numerical scheme can be written as

$$\begin{aligned} \rho_i^{n+1} &= \rho_i^n - \frac{k}{h} \left(f(u_{i+1/2}^n) - f(u_{i-1/2}^n) \right) \\ \alpha_i^{n+1} &= \alpha_i^n - \frac{k}{h} v(\rho_i^n, \alpha_i^n) (\alpha_i^n - \alpha_{i-1}^n), \end{aligned}$$

where $u_{i+1/2}$ is the solution of the Riemann problem with initial data u_i on $x < 0$ and u_{i+1} on $x \geq 0$ at $x = 0$. This value is uniquely defined by the above Riemann solver and thus u_i^{n+1} is uniquely defined for all $i \in \mathbb{Z}$ and $n \in \{0, \dots, N\}$. To obtain a stable method we impose the following relation between the space discretization h and the time step size k , known as CFL-condition.

$$k \leq \frac{1}{\|\partial_\alpha f\|_\infty + \alpha_{\max}} h \quad (8)$$

2.2.1. L^∞ bounds on ρ_i^n and α_i^n .

Lemma 2.1. *Let the CFL condition (8) hold. Furthermore, let $\rho(0, x)$ be given such that $0 \leq \rho(0, x) \leq 1$ a.e. in $[0, T] \times \mathbb{R}$ and $\alpha(0, x)$ such that $\alpha_{\min} \leq \alpha(0, x) \leq \alpha_{\max}$ a.e. in $[0, T] \times \mathbb{R}$. Then, for all $i \in \mathbb{Z}$ and all $n \in \{0, \dots, N\}$, the algorithm fulfills*

$$\begin{aligned} 0 &\leq \rho_i^n \leq 1 \\ \alpha_{\min} &\leq \alpha_i^n \leq \alpha_{\max}. \end{aligned}$$

Proof. Since $\rho(0, x)$ fulfills the constraint (5d), ρ_i^0 fulfills the same bounds by construction, see (7). The same holds true for α_i^0 .

We start with the estimate on α_i^n . Due to the construction of the Riemann solver, we have $\alpha_{i+1/2}^n = \alpha_i^n$ for all five cases of the above Riemann solver. According to the algorithm, we have therefore

$$\alpha_i^{n+1} = \alpha_i^n - \frac{k}{h} v_i^n (\alpha_i^n - \alpha_{i-1}^n) = (1 - \frac{k}{h} v_i) \alpha_i^n + \frac{k}{h} v_i^n \alpha_{i-1}^n.$$

The CFL condition assures that $(1 - \frac{k}{h} v_i)$ is positive and thus we conclude $\alpha_{\min} \leq \alpha_i^n \leq \alpha_{\max}$.

To show that the discrete solution fulfills the constraint $0 \leq \rho_i^n \leq 1$ at time $t^n > 0$, observe that $\rho_{i+1/2}^n = \rho_i^n$ or $\rho_{i+1/2}^n = \tilde{\rho}_i^n$, $\rho_{i+1/2}^n = \frac{1}{2}$ or $\rho_{i+1/2}^n = 0$ are the only possibilities admitted by the Riemann solver defined in Section 2.1. Therefore, we consider four cases, depending on the values of $\rho_{i+1/2}^n$ and $\rho_{i-1/2}^n$, the remaining cases being entirely similar:

Case 1. $\rho_{i+1/2}^n = \rho_i^n$ and $\rho_{i-1/2}^n = \rho_{i-1}^n$. Using the abbreviation $v_i^n := v(\rho_i^n, \alpha_i^n)$, we have

$$\begin{aligned} \rho_i^{n+1} &= \rho_i^n - \frac{k}{h} (f(\rho_i) - f(\rho_{i-1})) \\ &= \rho_i^n - \frac{k}{h} (\rho_i v_i^n - \rho_{i-1} v_{i-1}^n) \\ &= (1 - \frac{k}{h} v_i^n) \rho_i + \frac{k}{h} v_{i-1}^n \rho_{i-1} \\ &> 0, \end{aligned}$$

since the CFL condition (8) assures $0 \leq \frac{k}{h} v_i^n \leq 1$ for all $i \in \mathbb{Z}$ and $n \in \{0, \dots, N\}$. Therefore, we can estimate

$$\begin{aligned} \rho_i^{n+1} &= (1 - \frac{k}{h} v_i^n) \rho_i + \frac{k}{h} v_{i-1}^n \rho_{i-1} \\ &\leq \left(1 - \frac{k}{h} (v_i^n - v_{i-1}^n)\right) \|\rho^n\|_\infty. \end{aligned} \tag{9}$$

If $v_i^n \geq v_{i-1}^n$, we obtain $(1 - \frac{k}{h} (v_i^n - v_{i-1}^n)) < 1$ and (9) yields

$$\rho_i^{n+1} \leq \|\rho^n\|_\infty \leq 1.$$

However, if $v_i^n < v_{i-1}^n$, we cannot conclude the boundedness of ρ_i^{n+1} from (9). From the Riemann solver, we know that the case $v_i < v_{i-1}$ implies a shock wave connecting ρ_{i-1}^n and $\tilde{\rho}_{i-1}^n$, such that $\tilde{v}_{i-1}^n := v(\tilde{\rho}_{i-1}^n, \alpha_{i-1}^n) = v_i^n$. Since $\rho_{i-1/2}^n = \rho_{i-1}^n$, we can also conclude that the shock speed s_{i-1}^n is positive and by construction

$s_{i-1}^n < v_i$. Therefore, we rewrite (9)

$$\begin{aligned}\rho_i^{n+1} &= \rho_i^n - \frac{k}{h} (f(\rho_i) - f(\rho_{i-1})) \\ &= \rho_i^n - \frac{k}{h} (f(\rho_i) - f(\tilde{\rho}_{i-1}) + f(\tilde{\rho}_{i-1}) - f(\rho_{i-1})) \\ &= \rho_i^n - \frac{k}{h} (\rho_i^n v_i^n - \tilde{\rho}_{i-1}^n v_i^n + s_{i-1}^n (\tilde{\rho}_{i-1}^n - \rho_{i-1}^n)) \\ &= (1 - \frac{k}{h} v_i) \rho_i^n + \frac{k}{h} (v_i^n - s_{i-1}^n) \tilde{\rho}_{i-1}^n + \frac{k}{h} s_{i-1}^n \rho_{i-1}^n.\end{aligned}$$

The CFL condition (8) and $s_{i-1}^n < v_i^n$ assure now that all coefficients are positive. This together with the bound $\rho_{i-1}^n \leq \tilde{\rho}_{i-1}^n \leq 1$ yields

$$\rho_i^{n+1} \leq \left(1 - \frac{k}{h} v_i + \frac{k}{h} (v_i^n - s_{i-1}^n) + \frac{k}{h} s_{i-1}^n\right) = 1.$$

Case 2. $\rho_{i+1/2}^n = \rho_i^n$ and $\rho_{i-1/2}^n = \tilde{\rho}_{i-1}^n$. From $\tilde{v}_{i-1}^n = v_i^n$, we obtain directly

$$\begin{aligned}\rho_i^{n+1} &= \rho_i^n - \frac{k}{h} (f(\rho_i^n) - f(\tilde{\rho}_{i-1}^n)) \\ &= \rho_i^n - \frac{k}{h} (\rho_i^n v_i^n - \tilde{\rho}_{i-1}^n v_i^n) \\ &= (1 - \frac{k}{h} v_i^n) \rho_i^n + \frac{k}{h} v_i^n \tilde{\rho}_{i-1}^n.\end{aligned}$$

As in Case 1, CFL condition and bounds on ρ_i^n and $\tilde{\rho}_{i-1}^n$ assure $0 \leq \rho_i^{n+1} \leq 1$.

Case 3. $\rho_{i+1/2}^n = \tilde{\rho}_i^n$ and $\rho_{i-1/2}^n = \tilde{\rho}_{i-1}^n$. First, observe that we have

$$\begin{aligned}v_i^n - s_i^n &= \alpha_i^n (1 - \rho_i^n) - \alpha_i \frac{\tilde{\rho}_i^n (1 + \tilde{\rho}_i^n) - \rho_i^n (1 - \rho_i^n)}{\tilde{\rho}_i^n - \rho_i^n} \\ &= \alpha_i^n \frac{(1 - \rho_i^n)(\tilde{\rho}_i^n - \rho_i^n) - \tilde{\rho}_i^n (1 + \tilde{\rho}_i^n) + \rho_i^n (1 - \rho_i^n)}{\tilde{\rho}_i^n - \rho_i^n} \quad (10) \\ &= \alpha_i^n \tilde{\rho}_i^n\end{aligned}$$

and thus $0 \leq v_i^n - s_i^n \leq \alpha_i^n \leq \alpha_{\max}$. This yields

$$\begin{aligned}\rho_i^{n+1} &= \rho_i^n - \frac{k}{h} (f(\tilde{\rho}_i^n) - f(\tilde{\rho}_{i-1}^n)) \\ &= \rho_i^n - \frac{k}{h} (f(\tilde{\rho}_i^n) - f(\rho_i^n) + f(\rho_i^n) - f(\tilde{\rho}_{i-1}^n)) \\ &= \rho_i^n - \frac{k}{h} (s_i^n (\tilde{\rho}_i^n - \rho_i^n) + v_i^n (\rho_i^n - \tilde{\rho}_{i-1}^n)) \\ &= (1 - \frac{k}{h} (v_i^n - s_i^n)) \rho_i^n + \frac{k}{h} s_i^n \tilde{\rho}_i^n + \frac{k}{h} v_i^n \tilde{\rho}_{i-1}^n.\end{aligned}$$

Using (10), the CFL condition and the boundedness of $\tilde{\rho}_i^n$, we obtain $0 \leq \rho_i^{n+1} \leq 1$.

Case 4. $\rho_{i+1/2}^n = \tilde{\rho}_i^n$ and $\rho_{i-1/2}^n = \rho_{i-1}^n$. Here, we have

$$\rho_i^{n+1} = \rho_i^n - \frac{k}{h} (f(\tilde{\rho}_i^n) - f(\rho_{i-1}^n))$$

$$\begin{aligned}
&= \rho_i^n - \frac{k}{h} (f(\tilde{\rho}_i^n) - f(\rho_i^n) + f(\rho_i^n) - f(\rho_{i-1}^n)) \\
&= \rho_i^n - \frac{k}{h} (s_i^n (\tilde{\rho}_i^n - \rho_i^n) + \rho_i^n v_i^n - \rho_{i-1}^n v_{i-1}^n) \\
&= (1 - \frac{k}{h} (v_i^n - s_i^n)) \rho_i^n - \frac{k}{h} s_i^n \tilde{\rho}_i^n + \frac{k}{h} v_{i-1}^n \rho_{i-1}^n.
\end{aligned} \tag{11}$$

Since $\rho_{i+1/2}^n = \tilde{\rho}_i^n$, we can conclude $s_i^n < 0$. Again, using the CFL condition, equation (11) yields $\rho_i^{n+1} \geq 0$. Furthermore, if $v_i \geq v_{i-1}$, we also obtain the upper bound $\rho_i^{n+1} \leq 1$.

Now, assume $v_i < v_{i-1}$. Since $\rho_{i-1/2}^n = \rho_i^n$, we can conclude $s_{i-1}^n > 0$. Furthermore, $v_i^n > s_{i-1}^n$ by construction. Thus,

$$\begin{aligned}
\rho_i^{n+1} &= \rho_i^n - \frac{k}{h} (f(\tilde{\rho}_i^n) - f(\rho_{i-1}^n)) \\
&= \rho_i^n - \frac{k}{h} (f(\tilde{\rho}_i^n) - f(\rho_i^n) + f(\rho_i^n) - f(\tilde{\rho}_{i-1}^n) + f(\tilde{\rho}_{i-1}^n) - f(\rho_{i-1}^n)) \\
&= \rho_i^n - \frac{k}{h} (s_i^n (\tilde{\rho}_i^n - \rho_i^n) + v_i^n (\rho_i^n - \tilde{\rho}_{i-1}^n) + s_{i-1}^n (\tilde{\rho}_{i-1}^n - \rho_{i-1}^n)) \\
&= (1 - \frac{k}{h} (v_i^n - s_i^n)) \rho_i^n - \frac{k}{h} s_i^n \tilde{\rho}_i^n + \frac{k}{h} (v_i^n - s_{i-1}^n) \tilde{\rho}_{i-1}^n + \frac{k}{h} s_{i-1}^n \rho_{i-1}^n \\
&\leq 1.
\end{aligned}$$

The cases where $\rho_{i+1/2} = \frac{1}{2}$ and/or $\rho_{i-1/2} = \frac{1}{2}$ and the cases involving vacuum states follow in a similar way. \square

2.3. Effect of α on the solution. We show now the effect of α on the solution of model (5). Clearly, when α is homogeneous in space, the solution of (5) reduces to the solution of the classical LWR model. Thus, the initial condition $(\rho, \alpha_0)^T(0, x) := (\bar{\rho}, \bar{\alpha})^T$ yields $(\rho, \alpha_0)^T(t, x) := (\bar{\rho}, \bar{\alpha})^T$ constant in space and time. Now, we modify the initial condition and allow a space varying $\alpha(0, x)$ and use the velocity function $v(\rho, \alpha)$ given in (3) left with $\rho_{max} = 1$. The reference domain is formed by a strip of road of one kilometer length. Initially, $\alpha(0, x)$ is assumed to be piecewise constant on the intervals $[0.04(k-1), 0.04k]$, $k = 1, \dots, 25$, uniformly distributed in the interval $[25 \text{ m/s}, 30 \text{ m/s}]$. The inflow condition at the left boundary is chosen in a similar manner, such that α remains piecewise constant on strips of size 0.04 km . At the right boundary, we assume free outflow boundary conditions. Figure 3 shows the evolution of ρ and $v(\rho, \alpha)$ in time and space. One can observe that the evolution of ρ is not homogeneous, but shows regions of higher and lower density after short times. This effect coincides well with the observation of congestions that seem to appear out of nowhere in real traffic flow situations. In the model this is due to different velocities assigned to the same density according to the choice of α .

A similar but more pronounced behavior can be observed for higher initial densities, as shown in Figure 4.

Focusing on the trajectory of a car starting at time $t = 0$ at point $x = 0$, we observe that the driver sees a varying density and has to adjust his velocity accordingly, as shown in Figure 5. This behavior again matches the observations that can be experienced in real traffic flow situations, see e.g. [19, 20].

Finally, we focus on the variable α . By construction of the model and the scheme, α should stick to a specific car. Therefore it must be only transported by the flow and should not undergo any variation along a specific trajectory. Figure 6 shows

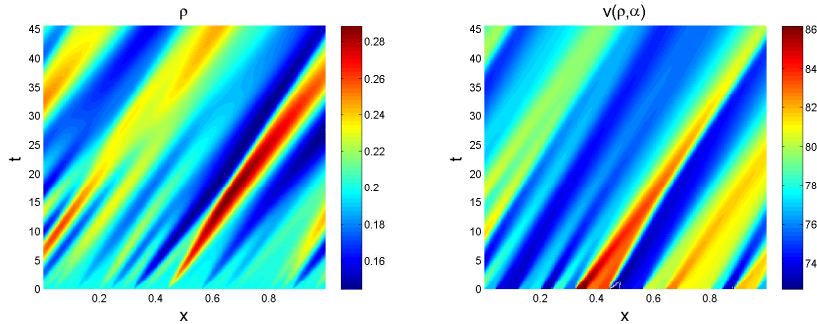


FIGURE 3. Evolution of ρ and $v(\rho, \alpha)$ [km/h] for a homogeneous initial density $\rho(0, x) = 0.2$. One can observe that regions of lower velocity (e.g. starting around $x = 0.5$) lead to an increasing density left of that region. This coincides with the observation of congestions that seem to appear from nowhere in real traffic flow situations.

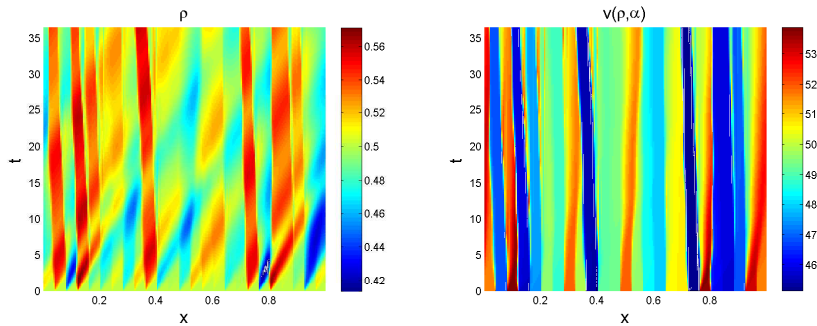


FIGURE 4. Evolution of ρ and $v(\rho, \alpha)$ [km/h] for a homogeneous initial density $\rho(0, x) = 0.5$. Again, regions of lower velocity cause high density regions to the left. Here the regions of varying density and velocity are nearly stationary in space and time.

that the numerical scheme fulfills this property, since $\alpha(t, x(t))$ is almost constant along the trajectory $(t, x(t))$ starting from $(0, 0)$. The small variations of α along the trajectory are due to the numerical diffusion introduced by the first order scheme.

To show the effect of the variable α on the outflow rate at the end of the street, we perform a Monte Carlo simulation with a sample size of 300, where the values of α on the intervals $[0.04(k-1), 0.04k]$, $k = 1, \dots, 25$ are distributed uniformly in $[20 \text{ m/s}, 40 \text{ m/s}]$. Figure 7 shows the distribution of the number of cars that exit the street in 10min. Using a constant value of $\alpha = 30 \text{ m/s}$ on the whole space-domain, 164 cars leave the street in 10 min, while the expected value using uniformly distributed values of α is given by 161 cars.

3. Generation of random initial data. In the case of traffic flow on roads or pedestrian movement, the exact position and often also the exact amount of cars or people in the domain under consideration cannot be known in advance. To compute

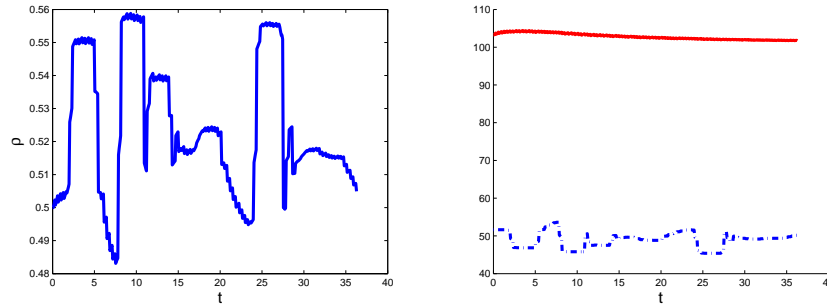


FIGURE 5. Evolution of $\rho(t, x(t))$ (left), $v(\rho(t, x(t)), \alpha(t, x(t)))$ (right, dashed blue) and $\alpha(t, x(t))$ (right, solid red) for a homogeneous initial density $\rho(0, x) = 0.5$ and $x(0) = 0$. One can observe that the driver encounters regions of higher and lower traffic density and has to adjust his velocity accordingly.

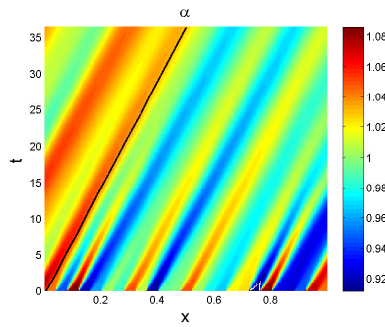


FIGURE 6. Evolution of α in space and time. The black line indicates the trajectory of a car starting at time $t = 0$ in position $x = 0$. One can observe that α remains almost constant along this trajectory as expected, due to the numerical viscosity of the scheme.

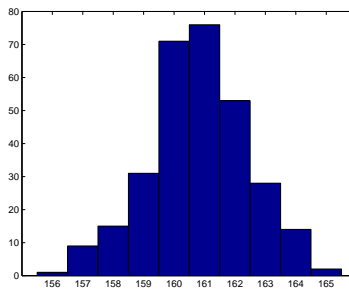


FIGURE 7. Statistical distribution of the number of cars that exit the street in a time interval of 10 *min*, using a homogeneous initial density of $\rho_0(x) = 0.5$.

some characteristic values like expected travel times or variations by Monte-Carlo type methods, we have to generate independent samples of admissible initial data.

Mathematically, this means that, given a domain $\mathcal{D} \subset \mathbb{R}^d$ and assuming we know the number M of objects in \mathcal{D} , we have to choose the initial distribution randomly from the set

$$\mathcal{M}(M) := \left\{ \rho \in \mathbf{L}^1(\mathcal{D}) \cap \mathbf{BV}(\mathcal{D}) \mid 0 \leq \rho \leq 1 \text{ a.e. in } \mathcal{D} \text{ and } \int_{\mathcal{D}} \rho \, dx = M \right\}.$$

In this formulation, ρ is given as number of objects per space unit (length or area). The generation of random initial data from this set is however mathematically difficult, as we are not able to define a valid probability measure on an infinite dimensional space (or a subset of it) and thus cannot give a meaning to notions such as expected value or variance. Therefore, we choose to generate initial data, following the underlying engineering context.

Assume that every object (car or person) occupies a space given by the ball $\mathcal{B}_{r,q}(\mathbf{p}_i) \subset \mathbb{R}^d$ of radius r in the q -Norm, centered around a midpoint $\mathbf{p}_i \in \mathbb{R}^d$. We define the matrix $\mathbf{p} \in \mathbb{R}^{d \times M}$, $(\mathbf{p})_{ji} = (\mathbf{p}_i)_j$ consisting of the midpoints of M objects. Then, the function

$$\rho_0(\mathbf{p}, x) = \sum_{i=1}^M \chi_{\mathcal{B}_{r,q}(\mathbf{p}_i)}(x), \quad (12)$$

indicates the space in \mathcal{D} that is occupied by M given objects located in the open balls $\mathcal{B}_{r,q}(\mathbf{p}_i)$ around the midpoints given in \mathbf{p} . Hereby, χ_I is the characteristic function, taking the value 1 on I and 0 outside I . To ensure that no two objects are in the same place, we require $\mathcal{B}_{r,q}(\mathbf{p}_i) \cap \mathcal{B}_{r,q}(\mathbf{p}_j) = \emptyset$ for all $i, j \in \{1, \dots, M\}$ with $i \neq j$. Thus, ρ_0 is given by an indicator function in the domain \mathcal{D} and fulfills the property $\int_{\mathcal{D}} \rho_0(x) \, dx = M |\mathcal{B}_{r,q}(0)|$. The above construction clearly guarantees $\rho_0 \in \mathbf{L}^1 \cap \mathbf{BV}$ and the normation of ρ_0 on the interval $[0, 1]$.

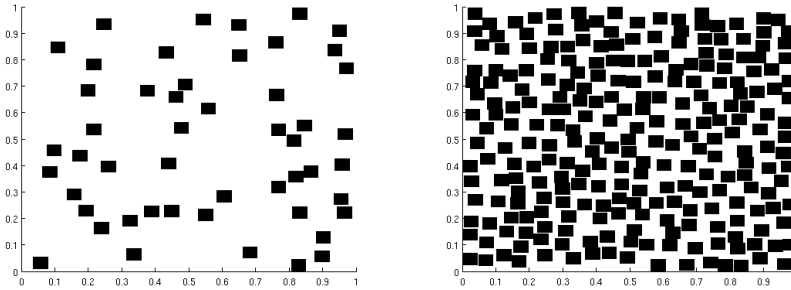


FIGURE 8. Two realizations of $\rho_0(\mathbf{p}, x)$ with $q = \infty$ and $r = \frac{1}{\sqrt{550}}$.
Left: $M = 50$. Right: $M = 250$.

Due to the construction, we can interpret \mathbf{p} as one elementary event from the set of all elementary events

$$\Omega := \left\{ A \in \mathbb{R}^{d \times M} \mid M \in \mathbb{N}, M |\mathcal{B}_{r,q}(0)| \leq |\mathcal{D}| \text{ and } |a_k - a_l|_q \geq 2r \right\}, \quad (13a)$$

where $a_k := (a_{i,k})_{i=1}^d$ is the k -th column of A .

In case M is fixed, we define instead

$$\Omega_M := \left\{ A \in \mathbb{R}^{d \times M} \mid |a_k - a_l|_q \geq 2r \right\}. \quad (13b)$$

Clearly, Ω and Ω_M are finite dimensional. Denoting by \mathcal{F} the corresponding σ algebra of all possible events, we can define the measurable spaces (Ω, \mathcal{F}) and $(\Omega_M, \mathcal{F}_M)$. Then, $\rho_0(\mathbf{p})$ can be interpreted as $\mathbf{L}^1(\mathcal{D})$ -valued random variable on (Ω, \mathcal{F}) or $(\Omega_M, \mathcal{F}_M)$. Assuming that all events in Ω are equally likely, ρ_0 is uniformly distributed.

Denoting by $(\Omega, \mathcal{F}, \mathbb{P})$ ($(\Omega_M, \mathcal{F}_M, \mathbb{P}_M)$) respectively the associated (complete) probability space, the expected value of ρ_0 , defined through

$$\mathbb{E}[\rho_0](x) = \int_{\Omega} \rho_0(\mathbf{p}, x) \mathbb{P}(d\mathbf{p})$$

is given by

$$\begin{aligned} \mathbb{E}[\rho_0](x) &= \frac{M}{|\mathcal{D}|} && \text{on } (\Omega_M, \mathcal{F}_M, \mathbb{P}_M) \\ \mathbb{E}[\rho_0](x) &= \frac{M^* + 1}{2|\mathcal{D}|} && \text{on } (\Omega, \mathcal{F}, \mathbb{P}) \end{aligned}$$

where $M^* := \left\lfloor \frac{|\mathcal{D}|}{|\mathcal{B}_{r,q}(0)|} \right\rfloor$ is the maximum number of objects that fit into the domain \mathcal{D} . Furthermore, ρ_0 is \mathbf{L}^1 -integrable and we have

$$\begin{aligned} \mathbb{E} [\|\rho_0\|_{\mathbf{L}^1(\mathcal{D})}] &= M |\mathcal{B}_{r,q}(0)| && \text{on } (\Omega_M, \mathcal{F}_M, \mathbb{P}_M) \\ \mathbb{E} [\|\rho_0\|_{\mathbf{L}^1(\mathcal{D})}] &= |\mathcal{B}_{r,q}(0)| \int_{\Omega} M(\mathbf{p}) \mathbb{P}(d\mathbf{p}) = |\mathcal{B}_{r,q}(0)| \mathbb{E}[M] && \text{on } (\Omega, \mathcal{F}, \mathbb{P}), \end{aligned}$$

where

$$\mathbb{E} [\|\rho_0\|_{\mathbf{L}^1(\mathcal{D})}] = \int_{\Omega} \|\rho_0(\mathbf{p}, \cdot)\|_{\mathbf{L}^1(\mathcal{D})} \mathbb{P}(d\mathbf{p}).$$

We use the framework provided by [16] and interpret $\rho_0 : (\Omega, \mathcal{F}) \rightarrow (\mathbf{L}^1(\mathcal{D}), \mathcal{B}(\mathbf{L}^1(\mathcal{D})))$ as $\mathbf{L}^1(\mathcal{D})$ -valued random variable, where $\mathcal{B}(I)$ denotes the Borel set of I . In the case, when M is fixed, we can analogously view $\rho_0 : (\Omega_M, \mathcal{F}_M) \rightarrow (\mathbf{L}^1(\mathcal{D}), \mathcal{B}(\mathbf{L}^1(\mathcal{D})))$ as $\mathbf{L}^1(\mathcal{D})$ -valued random variable.

Define now the Bochner norms

$$\begin{aligned} \|\rho\|_{\mathbf{L}^k(\Omega; \mathbf{L}^1(\mathcal{D}))} &:= \left(\int_{\Omega} \|\rho_0\|_{\mathbf{L}^1(\mathcal{D})}^k \mathbb{P}(d\mathbf{p}) \right)^{\frac{1}{k}} && \text{for } 1 \leq k < \infty \\ \|\rho\|_{\mathbf{L}^\infty(\Omega; \mathbf{L}^1(\mathcal{D}))} &:= \operatorname{ess\,sup}_{\mathbf{p} \in \Omega} \|\rho_0(\mathbf{p}, \cdot)\|_{\mathbf{L}^1(\mathcal{D})} \end{aligned}$$

and the associated Bochner spaces

$$L^k(\Omega; \mathbf{L}^1(\mathcal{D})) := \{ \rho : (\Omega, \mathcal{F}) \rightarrow (\mathbf{L}^1(\mathcal{D}), \mathcal{B}(\mathbf{L}^1(\mathcal{D}))) \mid \|\rho\|_{\mathbf{L}^k(\Omega; \mathbf{L}^1(\mathcal{D}))} < \infty \}.$$

Lemma 3.1. *Let ρ_0 be defined as in (12) and Ω, Ω_M be given as in (13a), (13b). Then, ρ_0 fulfills the k th moment condition*

$$\|\rho_0\|_{\mathbf{L}^k(\Omega; \mathbf{L}^1(\mathcal{D}))} < \infty \quad \text{and} \quad \|\rho_0\|_{\mathbf{L}^k(\Omega_M; \mathbf{L}^1(\mathcal{D}))} < \infty. \quad (14)$$

for all $k \in \mathbb{N}$.

Proof. Indeed, it is easy to see that we have for $k \in \mathbb{N}$

$$\begin{aligned} \|\rho_0\|_{\mathbf{L}^k(\Omega_M; \mathbf{L}^1(\mathcal{D}))}^k &= \int_{\Omega_M} \|\rho_0(\mathbf{p}, \cdot)\|_{\mathbf{L}^1(\mathcal{D})}^k \mathbb{P}(d\mathbf{p}) \\ &= \int_{\Omega_M} (M |\mathcal{B}_{r,q}(0)|)^k \mathbb{P}(d\mathbf{p}) \\ &= (M |\mathcal{B}_{r,q}(0)|)^k < \infty. \end{aligned}$$

Furthermore,

$$\begin{aligned} \|\rho_0\|_{\mathbf{L}^k(\Omega, \mathbf{L}^1(\mathcal{D}))}^k &= \int_{\Omega} \|\rho_0(\mathbf{p}, \cdot)\|_{\mathbf{L}^1(\mathcal{D})}^k \mathbb{P}(d\mathbf{p}) \\ &= \int_{\Omega} (M(\mathbf{p})|\mathcal{B}_{r,q}(0)|)^k \mathbb{P}(d\mathbf{p}) \\ &= (|\mathcal{B}_{r,q}(0)|)^k \int_{\Omega} (M(\mathbf{p}))^k \mathbb{P}(d\mathbf{p}) \\ &= (|\mathcal{B}_{r,q}(0)|)^k \mathbb{E}[M^k]. \end{aligned}$$

$M(\mathbf{p})$ is a random variable with values in a finite set, since $M \in \{1, \dots, M^*\}$, such that $\mathbb{E}[M^k] \leq \sum_{m=1}^{M^*} m^k$ is finite for all $k \in \mathbb{N}$. \square

To use the α -model (4), we need to specify a value of $\alpha \in [\alpha_{\min}, \alpha_{\max}]$ for each object \mathbf{p}_i . This can be easily obtained by a small modification of Ω and Ω_M .

$$\Omega := \left\{ A \in \mathbb{R}^{(d+1) \times M} \left| \begin{array}{l} M \in \mathbb{N}, M|\mathcal{B}_{r,q}(0)| \leq |\mathcal{D}|, (a_i k)_{i=1}^d \in \mathcal{D} \\ |(a_i k)_{i=1}^d - (a_i l)_{i=1}^d|_q \geq 2r \text{ and } a_{d+1,k} \in [\alpha_{\min}, \alpha_{\max}] \end{array} \right. \right\},$$

where $a_k := (a_{ik})_{i=1}^d$ is the k -th column of A without the last line, that corresponds to the initial value of α assigned to object k .

In case M is fixed, we get instead

$$\Omega := \left\{ A \in \mathbb{R}^{(d+1) \times M} \left| \begin{array}{l} (a_i k)_{i=1}^d \in \mathcal{D}, |(a_i k)_{i=1}^d - (a_i l)_{i=1}^d|_q \geq 2r \\ \text{and } a_{d+1,k} \in [\alpha_{\min}, \alpha_{\max}] \end{array} \right. \right\}.$$

Analogously to ρ_0 above, we can now define α_0 as piecewise constant function. In principle, α can be chosen arbitrarily in all regions of the initial data, where $\rho_0(x) = 0$, as it does not affect the solution by construction of the Riemann solver. Recall that α_{\pm} is not used in the Riemann solver, when the data contains vacuum states. However, for computational reasons it is useful to choose α in one of the following ways, according to the application:

- The choice of $\alpha = \alpha_{\max}$ in all regions where $ho_0 = 0$ is numerically advantageous, since it avoids some case distinctions.
- However, if the expected value of α is needed (e.g. for comparison with a deterministic model), the choice $\alpha = \mathbb{E}[\alpha]$ in all regions where $\rho_0 = 0$ conserves the numerical expected value of α .

4. Application to crowd dynamics. In this section, we compare the model (1) with the α -model (2), augmented by the additional equation for α . To start, we review some results on existence and continuous dependence of solutions for model (1), that can be found in [5].

Definition 4.1. Let $T > 0$ and $\rho_{\max} > 0$ be fixed and choose $\rho_0 \in \mathbf{L}^1(\mathbb{R}^d; [0, \rho_{\max}])$. A function $\rho \in \mathbf{C}^0([0, T]; \mathbf{L}^1(\mathbb{R}^d; \mathbb{R}))$ is a weak solution to the Cauchy problem

$$\begin{aligned} \partial_t \rho + \mathbf{div}(\rho v(\rho)(\boldsymbol{\nu}(x) - \varepsilon \mathcal{I}(\nabla \eta * \rho))) &= 0 \\ \rho(0, x) &= \rho_0(x) \end{aligned}$$

if it is a solution to

$$\begin{aligned} \partial_t \rho + \mathbf{div}(\rho v(\rho) \mathbf{w}(t, x)) &= 0 \\ \rho(0, x) &= \rho_0(x) \end{aligned}$$

in the sense of Kruřkov (see [14]) with $\mathbf{w}(t, x) = \boldsymbol{\nu}(x) - \varepsilon \mathcal{I}(\nabla \eta * \rho)$.

Before we recall the existence result, we have to impose additional assumptions of the vector field ν and the non local term \mathcal{I} .

- (ν) $\nu \in (\mathbf{C}^2 \cap \mathbf{W}^{1,\infty})(\mathbb{R}^d; \mathbb{R}^d)$ fulfills $\operatorname{div} \nu \in (\mathbf{W}^{1,1} \cap \mathbf{W}^{1,\infty})(\mathbb{R}^d; \mathbb{R})$.
- (\mathcal{I}) $\mathcal{I} \in \mathbf{C}^0(\mathbf{L}^1(\mathbb{R}^d; [0, \rho_{\max}]); \mathbf{C}^2(\mathbb{R}^d; \mathbb{R}^d))$ and there exists an increasing function $C_{\mathcal{I}} \in \mathbf{L}_{loc}^\infty(\mathbb{R}^+, \mathbb{R}^+)$ and a constant $K_{\mathcal{I}}$ such that \mathcal{I} fulfills the following estimates for all $r, r_1, r_2 \in \mathbf{L}^1(\mathbb{R}^d, [0, \rho_{\max}])$:
 - (a) $\|\mathcal{I}(r)\|_{\mathbf{W}^{1,\infty}} \leq C_{\mathcal{I}}(\|r\|_{\mathbf{L}^1})$
 - (b) $\|\operatorname{div} \mathcal{I}(r)\|_{\mathbf{L}^1} \leq C_{\mathcal{I}}(\|r\|_{\mathbf{L}^1})$
 - (c) $\|\nabla \operatorname{div} \mathcal{I}(r)\|_{\mathbf{L}^1} \leq C_{\mathcal{I}}(\|r\|_{\mathbf{L}^1})$
 - (d) $\|\mathcal{I}(r_1) - \mathcal{I}(r_2)\|_{\mathbf{L}^\infty} \leq K_{\mathcal{I}}\|r_1 - r_2\|_{\mathbf{L}^1}$
 - (e) $\|\mathcal{I}(r_1) - \mathcal{I}(r_2)\|_{\mathbf{L}^1} + \|\operatorname{div}(\mathcal{I}(r_1) - \mathcal{I}(r_2))\|_{\mathbf{L}^1} \leq K_{\mathcal{I}}\|r_1 - r_2\|_{\mathbf{L}^1}$

With these assumptions, the authors of [5] proof existence, uniqueness and continuous dependence of the solution from the initial data and obtain the following result.

Theorem 4.2. *Let (\mathbf{v}) , (ν) and (\mathcal{I}) hold and choose $\rho_0 \in (\mathbf{L}^1 \cap \mathbf{BV})(\mathbb{R}^d; [0, \rho_{\max}])$. Then, there exists a unique entropy solution $\rho \in \mathbf{C}^0(\mathbb{R}^+; \mathbf{L}^1(\mathbb{R}^d; [0, \rho_{\max}]))$ to (1). Moreover, $\rho(t) = F(t)\rho_0$ satisfies*

$$\|F(t)\rho_0\|_{\mathbf{L}^1} = \|\rho_0\|_{\mathbf{L}^1} \quad \text{for a. e. } t \in \mathbb{R}^+. \tag{15}$$

For $\rho_{0,1}, \rho_{0,2} \in (\mathbf{L}^1 \cap \mathbf{BV})(\mathbb{R}^d; [0, \rho_{\max}])$, the two solutions of (1) satisfy

$$\|F(t)\rho_{0,1} - F(t)\rho_{0,2}\|_{\mathbf{L}^1} \leq C(t)\|\rho_{0,1} - \rho_{0,2}\|_{\mathbf{L}^1}$$

where F denotes the solution operator in time.

Note that the result in [5] also includes a total variation bound for $\rho(t)$ and continuous dependence of the solution on ν , the speed law v and the non local term \mathcal{I} . In the simulation below, we use

$$\mathcal{I}(\nabla \eta * \rho) = \frac{\nabla \eta * \rho}{\sqrt{1 - \|\nabla \eta * \rho\|^2}},$$

which was proved to fulfill the assumptions (\mathcal{I}) in [5].

Concerning the numerical solution of (1), a Lax-Friedrichs type method was proposed in [1] in one space dimension and it seems possible to extend the convergence result therein to the two dimensional case, using the dimensional splitting approach proposed in [7]. Therefore, we use this approach as numerical scheme for model (1).

To compare the results of (1) and (2), we use random initial data generated by the method proposed in section 3. Recently, Mishra and Schwab proposed a theoretical framework [16] to deal with conservation laws with random initial data. Therein, the authors proof the measurability of the mapping $\mathbf{p} \mapsto S(t)\rho_0(\cdot, \mathbf{p})$ under standard assumptions on the solution $S(t)\rho_0$ of a single conservation law in d space dimensions. We adapt the result [16, Theorem 3.3] to the present setting and obtain

Theorem 4.3. *Let (\mathbf{v}) , (ν) and (\mathcal{I}) hold and choose $\rho_0 : \Omega \rightarrow (\mathbf{L}^1 \cap \mathbf{BV})(\mathbb{R}^d; [0, \rho_{\max}])$ such that ρ_0 fulfills the k -th moment condition (14) for some $k \in \mathbb{N}$. Then, there exists a unique random entropy solution $\rho : \Omega \ni \mathbf{p} \rightarrow \mathbf{C}^0([0, T]; \mathbf{L}^1(\mathbb{R}^d; [0, \rho_{\max}]))$ given by $\rho(\cdot, t, \mathbf{p}) = F(t)\rho_0(\cdot, \mathbf{p})$. Moreover, for every $k \geq m \geq 1$ and almost every $0 \leq t \leq T$, we have \mathbb{P} -almost surely*

$$\|\rho\|_{\mathbf{L}^m(\Omega; \mathbf{C}^0([0, T]; \mathbf{L}^1(\mathbb{R}^d)))} = \|\rho_0\|_{\mathbf{L}^m(\Omega; \mathbf{L}^1(\mathbb{R}^d))}. \tag{16}$$

Hereby, $\|\rho\|_{\mathbf{L}^m(\Omega; \mathbf{C}^0([0,T]; \mathbf{L}^1(\mathbb{R}^d)))}^m := \int_{\Omega} (\max_{0 \leq t \leq T} \|F(t)\rho_0(\cdot, \mathbf{p})\|_{\mathbf{L}^1})^m d\mathbb{P}(\mathbf{p})$. The proof of this result is entirely analogous to the proof in [16], using the equality (15). An analogous result holds for Ω_M instead of Ω . Note that the method to generate random initial conditions proposed in Section 3 guarantees that ρ_0 fulfills the k -th moment condition, as shown in Lemma 3.1. Thus, the k -th moment of the solution is well-defined, especially the expected value of $\|\rho\|_{\mathbf{L}^1(\mathbb{R}^d)}$ at any given time $T > 0$. Since the relation (16) holds only on the whole domain \mathbb{R}^d , we use a standard Monte Carlo method to approximate the expected value of $\|\rho(T)\|_{\mathbf{L}^1}$ in the bounded domain \mathcal{D} , which is given by $\mathbb{E}[\rho(T)] = \|\rho(T)\|_{\mathbf{L}^1(\Omega; \mathbf{L}^1(\mathcal{D}; [0, \rho_{\max}]))}$.

Turning now to the α -model (2), we cannot rely on a thorough theoretical background, as no results are available for systems of conservation laws in more than one space dimension. This implies also that we do not have any formal knowledge if the expected value of $\|\rho(T)\|_{\mathbf{L}^1(\mathbb{R}^d)}$ is well defined for model (2).

For the numerical simulation of the α -model (2), we use a dimensional splitting (see [7]) based on the algorithm proposed in Section 2.2, now modified to take into account the convolution term as time and space dependent contribution to the flux.

For the numerical comparison, we use the following setting. The domain \mathcal{D} is given by a room of size of 20 m \times 20 m, initially filled with 600 persons distributed randomly, using the method described in Section 3. The basic directional field ν is given by the normed solution of the eikonal equation, with boundary conditions corresponding to a door at $x = 20$ m, $y \in [6$ m, 12 m], see Figure 9 as well as [18] for a description of the numerical algorithm used to compute the vector field.

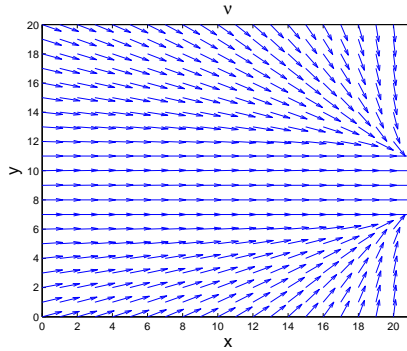


FIGURE 9. Directional field ν for the simulation of the evacuation scenario.

We assume that the maximal density ρ_{\max} is given by 5.5 people per square meter, where each person occupies a square space of size $\frac{1}{\rho_{\max}}$. This yields an absolute maximum of 1100 persons that fit into the room, when no empty space is left between the individuals. Thus, the initial distribution of 600 persons in the room corresponds to a rather crowded scenario.

The velocity functions are chosen as

$$\begin{aligned} v(\rho) &= v_{\max} \left(1 - \frac{\rho}{\rho_{\max}}\right), & v_{\max} &= \frac{5 \text{ m}}{3.6 \text{ s}} \\ v(\rho, \alpha) &= \alpha \left(1 - \frac{\rho}{\rho_{\max}}\right), & \alpha &\in \left[\frac{3 \text{ m}}{3.6 \text{ s}}, \frac{7 \text{ m}}{3.6 \text{ s}} \right], \end{aligned}$$

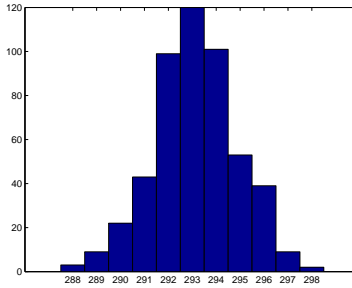


FIGURE 10. Statistical distribution of the number of people remaining inside the room for a given deterministic initial condition $\rho_0(x)$ and uniformly distributed α_0 .

what corresponds to a mean velocity of $5 \frac{\text{km}}{\text{h}}$ or 3.11 mph and a spread between $3 \frac{\text{km}}{\text{h}}$ and $7 \frac{\text{km}}{\text{h}}$ or 1.87 mph and 4.35 mph. For each position \mathbf{p}_i the associated individual maximum speed α_i is given by a uniformly distributed random variable with values in $[3, 7]$;

Concerning the non local term \mathcal{I} , we use a gaussian kernel, given by

$$\eta(x, y) = \frac{\sigma}{2\pi} e^{-\frac{\sigma}{2}(x^2+y^2)}$$

with $\sigma = 500$. The scaling for \mathcal{I} is chosen as $\varepsilon = 0.1$.

The numerical simulation is performed on a regular grid of 40×40 cells up to time $T = 30s$. In a first test case, we use the same initial data ρ_0 for all 500 samples of the Monte Carlo simulation, with varying α_0 , uniformly distributed in the interval $[3, 7]$ to illustrate the effect of the additional equation on the solution. Figure 10 shows the distribution of the number of people remaining in the room after 30s. The expected value of the number of people remaining inside computed through this Monte Carlo-simulation is given by ≈ 293.14 , while the deterministic model with $v_{\max} = 5$ yields ≈ 293.13 persons remaining inside. As a second example, we estimate the expected value of $\|\rho(T)\|_{\mathbf{L}^1(\mathcal{D})}$, using a sample size of 500. Figure 11 shows the distribution of the number of people remaining inside the room after 30s for both models. From this result one can clearly see that less persons left the room, when the simulation is performed with the α -model (2). Furthermore, the variance of the distribution resulting from (2) is higher than the variance of the distribution resulting from the original model (1). In Figure 12, we show the evolution of the expected value with increasing sample size. This emphasizes that the expected amount of people evacuated from the room is lower for the α -model (2).

5. Conclusion. We presented a new model that can be applied to traffic flow and crowd dynamics problems and takes into account the statistical variability of maximal speeds of different persons or cars/drivers respectively. The proposed numerical method for the solution of this new model was shown to respect the bounds on density and velocity. Numerical experiments in one space dimension showed that the model is capable to produce regions of higher and lower density even when starting from homogeneous initial densities. This behavior is in accordance with observations in real traffic flow situations. A comparison of the behavior of the new model and an established model showed that the new model leads to lower

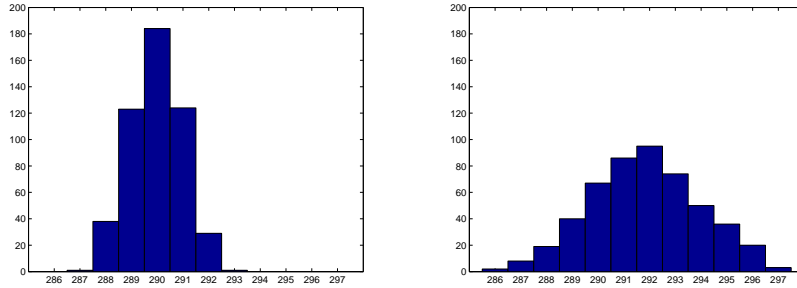


FIGURE 11. Statistical distribution of the number of people remaining inside the room after 30 s. Left: Model (1). Right: The new α -model (2).

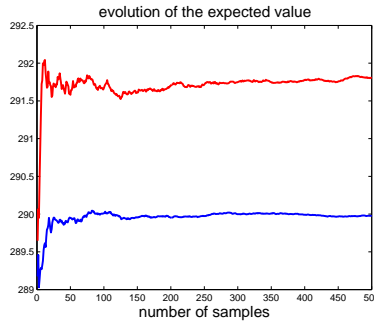


FIGURE 12. Evolution of the expected values of the number of people remaining in the room after 30 s for increasing sample size. Blue: Model (1). Red: The new α -model (2).

evacuation speeds due to the presence of varying maximal velocities, even though the expected value of the maximal velocity in regions of positive density was equal to the one used for the established model.

Acknowledgments. The author would like to thank the organizers and participants of the Workshop *Modeling with Measures: from Structured Populations to Crowd Dynamics* held from 26 Aug 2013 through 30 Aug 2013 at the Lorenz center in Leiden, Netherlands, for the inspring discussions and suggestions.

REFERENCES

- [1] P. Amorim, R. M. Colombo and A. Teixeira, On the numerical integration of scalar conservation laws, preprint, 2013.
- [2] A. Aw and M. Rascle, [Resurrection of “second order” models of traffic flow](#), *SIAM J. Appl. Math.*, **60** (2000), 916–938 (electronic).
- [3] N. Bellomo and C. Dogbé, [On the modelling crowd dynamics from scaling to hyperbolic macroscopic models](#), *Math. Models Methods Appl. Sci.*, **18** (2008), 1317–1345.
- [4] N. Bellomo and C. Dogbé, [On the modeling of traffic and crowds: A survey of models, speculations, and perspectives](#), *SIAM Review*, **53** (2011), 409–463.
- [5] R. M. Colombo, M. Garavello and M. Lécureux-Mercier, [A class of non-local models for pedestrian traffic](#), *Mathematical Models and Methods in the Applied Sciences*, **22** (2012), 1150023, 34 p.

- [6] R. M. Colombo and N. Pogodaev, [Confinement strategies in a model for the interaction between individuals and a continuum](#), *SIAM J. Appl. Dyn. Syst.*, **11** (2012), 741–770.
- [7] M. Crandall and A. Majda, [The method of fractional steps for conservation laws](#), *Numer. Math.*, **34** (1980), 285–314.
- [8] E. Cristiani, B. Piccoli and A. Tosin, [Multiscale modeling of granular flows with application to crowd dynamics](#), *Multiscale Model. Simul.*, **9** (2011), 155–182.
- [9] C. F. Daganzo, [Requiem for second-order fluid approximations to traffic flow](#), *Transp. Res. B*, **29** (1995), 277–286.
- [10] G. Dal Maso, P. G. Lefloch and F. Murat, [Definition and weak stability of nonconservative products](#), *J. Math. Pures Appl. (9)*, **74** (1995), 483–548.
- [11] D. Helbing, [Derivation of non-local macroscopic traffic equations and consistent traffic pressures from microscopic car-following models](#), *The European Physical Journal B*, **69** (2009), 539–548.
- [12] D. Helbing and A. F. Johansson, [On the controversy around Daganzo’s requiem for and Aw-Rascle’s resurrection of second-order traffic flow models](#), *Modelling and Optimisation of Flows on Networks*, (2013), 271–302.
- [13] R. L. Hughes, [A continuum theory for the flow of pedestrians](#), *Transportation Research Part B: Methodological*, **36** (2002), 507–535.
- [14] S. N. Kruzhkov, [First order quasilinear equations with several independent variables](#), *Mat. Sb. (N.S.)*, **81** (1970), 228–255.
- [15] M. J. Lighthill and G. B. Whitham, [On kinematic waves. II. A theory of traffic flow on long crowded roads](#), *Proc. Roy. Soc. London. Ser. A.*, **229** (1955), 317–345.
- [16] S. Mishra and C. Schwab, [Sparse tensor multi-level Monte Carlo finite volume methods for hyperbolic conservation laws with random initial data](#), *Math. Comp.*, **81** (2012), 1979–2018.
- [17] P. I. Richards, [Shock waves on the highway](#), *Operations Res.*, **4** (1956), 42–51.
- [18] M. Sabry Hassouna and A. A. Farag, [Multistencils fast marching methods: A highly accurate solution to the eikonal equation on cartesian domains](#), *IEEE Transactions on Pattern Analysis and Machine Intelligence*, **29** (2007), 1563–1574.
- [19] Y. Sugiyama, M. Fukui, M. Kikuchi, K. Hasebe, A. Nakayama, K. Nishinari, S.-i. Tadaki and S. Yukawa, [Traffic jams without bottlenecks—experimental evidence for the physical mechanism of the formation of a jam](#), *New Journal of Physics*, **10** (2008), 033001.
- [20] S.-i. Tadaki, M. Kikuchi, F. Minoru, A. Nakayama, K. Nishinari, A. Shibata, Y. Sugiyama, T. Yosida and S. Yukawa, [Phase transition in traffic jam experiment on a circuit](#), *New Journal of Physics*, **15** (2013), 103034.

Received April 24, 2014; Accepted June 27, 2014.

E-mail address: veronika.schleper@mathematik.uni-stuttgart.de